

Biomaterials Processing

biomaterials applications

Journal of Biomaterials Applications 2020, Vol. 34(10) 1368–1380 © The Author(s) 2020 Article reuse guidelines: sagepub.com/journals-permissions DOI: 10.1177/0885328220905103 journals.sagepub.com/home/jba



Antibacterial activities and cell responses of Ti-Ag alloys with a hybrid micro- to nanostructured surface

Zeming Lei^{1,2}, Hangzhou Zhang³, Erlin Zhang⁴, Junhua You⁵, Xiaoxue Ma⁶ and Xizhuang Bai² ®

Abstract

In this study, the surfaces of Ti–Ag casting alloys were modified by chemical treatment (acid etching combined with alkaline treatment) to produce hybrid micron and submicron porosities, sponge-like nanostructures and Ag-containing particles. The surface characteristics, ion release, pH values, antibacterial activities and cell responses of the chemically treated Ti–Ag (Ti–Ag(CT)) samples were investigated. The antibacterial activities of the Ti–Ag(CT) samples were assessed using Staphylococcus aureus, and these samples showed strong antibacterial activities that were attributed to Ag ion release and Ag-containing particles. The effects of Ti–Ag(CT) samples on cells were assessed using MC3T3-EI mouse preosteoblasts; samples with I and 3 wt.% Ag showed higher cell adhesion and higher alkaline phosphatase values than those of commercially available pure Ti samples. These results indicated that Ti–Ag casting alloys with I and 3 wt.% Ag modified by chemical treatment prevented bacterial infection and have latent capacities to promote osseointegration.

Keywords

Titanium, silver, chemical treatment, antibacterial property, cell response

Introduction

Titanium (Ti) and Ti-based alloys have been widely used as joint prostheses for many years due to their excellent biocompatibility, low modulus and enhanced corrosion resistance. However, the rates of prosthetic joint infection (PJI) and aseptic loosening are the two main challenges of using joint arthroplasty prostheses. While the infection rate varies depending on the joint replaced, it has been evaluated and ranges from 0.39 to 2.5% after primary total knee arthroplasty (TKA) and from 1 to 2% after primary total hip arthroplasty (THA).² Additionally, aseptic loosening is the most common cause of revision TKA and revision THA, accounting for 29.8% of revision TKAs and 55.2% of revision THAs.³ The pathogenesis of PJI consists of bacterial adhesion and proliferation and subsequent biofilm formation, whereas failure in osseointegration can result in aseptic loosening. 4,5 Therefore, there is an urgent need to design a Ti-based alloy that can simultaneously prevent PJI and still promote osseointegration.

To obtain antibacterial properties, silver (Ag) has been applied as an inorganic antibacterial element in antibacterial materials, even in the clinic, due to its strong antibacterial ability, broad antimicrobial spectrum, small chance for developing resistant bacteria and low cytotoxicity. ^{6–10} However, an as-cast Ti–Ag alloy only suppressed biofilm formation and was not

¹Hand Surgery Ward, Central Hospital Attached to Shenyang Medical College, Shenyang, China

²Department of Orthopedics and Sports Medicine and Joint Surgery, The People's Hospital of China Medical University, Shenyang, China

³Department of Orthopedics and Sports Medicine and Joint Surgery, The First Affiliated Hospital of China Medical University, Shenyang, China

⁴Key Laboratory for Anisotropy and Texture of Materials (ATM),

Education Ministry of China, School of Material Science and Engineering, Northeastern University, Shenyang, China

⁵School of Materials Science and Engineering, Shenyang University of Technology, Shenyang, China

⁶Department of Medical Microbiology and Parasitology, College of Basic Medical Sciences, China Medical University, Shenyang, China

Corresponding authors:

Zeming Lei, Hand Surgery Ward, Central Hospital Attached to Shenyang Medical College, Department of Orthopedics and Sports Medicine and Joint Surgery, The People's Hospital of China Medical University, Shenyang, China.

Email: leizem@163.com

Xizhuang Bai, Department of Orthopedics and Sports Medicine and Joint Surgery, The People's Hospital of China Medical University, Shenyang, China.

Email: bai_xizhuang@sina.com

bactericidal when the concentration of added Ag was as high as 20 wt.%. Then et al. 12 used heat treatment to prepare Ti₂Ag precipitate from a Ti-15 wt.% Ag casting alloy. The Ti-15 wt.% Ag casting alloy was prepared by a casting and heat treatment method and exhibited a 99.99% antibacterial rate. Ti₂Ag had a significant impact on antibacterial activities; however, the amount of added Ag was still too high, resulting in a high production cost. Apart from the casting method, powder metallurgy was used to make a Ti–Ag alloy with a smaller amount of Ag (3 wt.%) that achieved a good antibacterial ratio (AR) (98.2%), but the Ti–Ag-sintered alloy had much lower ductility, making it not well suited for joint prostheses. 13

Although the abovementioned Ti-Ag alloys showed different degrees of antibacterial abilities, they lacked the ability to promote osseointegration. Sandblasting and acid etching (SLA) is a popular surface treatment method to improve osseointegration.¹⁴ Kang et al.¹⁵ found that Ti-Ag casting alloys with low Ag contents (1-4 wt.%) treated by SLA exhibited good ARs (>90%) and were biocompatible, but their cell response and osseointegration were not tested. Traditional SLA can promote osteoblast differentiation; nevertheless, the traditional SLA surface, which is hydrophobic, has no positive effects on cell adherence and proliferation. ^{16–19} The surface of Ti-based materials modified by chemical treatment (CT, acid etching plus alkaline treatment) can have hybrid micro-, submicro- and nanostructures and has been proven to be highly hydrophilic and to promote bone-related gene expression, hydroxyapatite deposition and new bone formation. 20,21 Moreover, compared with other modification methods, CT inexpensive, effective and reproducible.

Therefore, in this work, we fabricated a Ti–Ag alloy with a hybrid micro- to nanostructured surface to address PJI and aseptic loosening in the clinic. This alloy has broad clinical prospects and great market potential. To endow titanium with the necessary antibacterial properties, Ag was added to Ti; subsequently, Ti–Ag alloys were prepared by the casting method. Moreover, to minimize the costs, we limited the silver content of the titanium silver alloys no higher than 5 wt.%. To promote osseointegration, Ti–Ag alloy substrates were modified by CT to generate hydrophilic surfaces with hybrid micro-, submicro- and nanostructures. The surface characteristics, antibacterial activities and preosteoblastic cell responses of the samples were systematically investigated.

Furthermore, the Ti–Ag alloy used in this study comprises innovative properties compared with those of other studies. ^{11–13,15,22} First, the hybrid micro- to nanostructured surfaces exhibited antibacterial properties at low silver concentrations. Second, the modified

alloy also showed better cell responses in adhesion and osteogenic differentiation. Third, the preparation and surface modification of the Ti–Ag alloy with hybrid micro- to nanostructured surfaces were uncomplicated and feasible.

Materials and methods

Sample preparation

Commercially available pure Ti (cp-Ti) and high-purity Ag were fabricated by vacuum melting in a nonconsumable furnace to prepare Ti-Ag alloys with 1, 3 and 5 wt.% Ag. An ingot was melted at least six times. Cp-Ti and Ti-Ag alloy slices were cut into thin plates with a diameter of 15 mm and a thickness of 2 mm, ground with SiC paper of up to 2000 grit and sequentially cleaned in acetone, alcohol and deionized water. The CT included two steps. In the acid etching step, all samples were immersed in 2 M HCl solution for 2 h at 60°C (named Ti(AE), Ti-1Ag(AE), Ti-3Ag(AE) and Ti-5Ag(AE)) and subsequently treated in 5 M NaOH solution for 24 h at 60°C (named Ti(CT), Ti-1Ag(CT), Ti-3Ag(CT) and Ti-5Ag(CT)). Afterwards, the samples were ultrasonically cleaned three times in ultrapure water for 30 min.

Sample characterization

Field emission scanning electron microscopy (FE–SEM, GeminiSEM300, ZEISS, Germany) with energy-dispersive X-ray spectroscopy (EDS) was performed to observe the surface morphology and the Ag content on sample surfaces. Phase identification was investigated by X-ray diffraction (XRD, D/max2400, Rigaku, Japan). The surface roughness was determined using confocal laser scanning microscopy (Lext Ols4100, Olympus Corporation, Japan). The water contact angle was determined (SL200KS, Kino Industry Corporation, Ltd, USA) using distilled water.

Ag ion release and pH measurements

Each Ti–Ag sample was immersed in 1.5 mL of 0.9% NaCl solution at 37 °C for 28 days, and the solution was changed daily to simulate the physiological environment inside the human body. The surface areato-volume ratio was approximately 3.0 according to the standard ISO 10993-12.²³ The Ag ions of the solution on days 1, 4, 7, 14 and 28 were quantified by inductively coupled plasma mass spectrometry (ICP–MS, 7700x, Agilent, USA). The pH values of the solution were analysed for 24 h by a pH meter (PHS-3C, Shanghai INESA Scientific Instrument Co., Ltd, China).

In vitro antibacterial assays

Bacterial culture. Staphylococcus aureus (S. aureus) strain ATCC6538 (American Type Culture Collection, USA) was used in in vitro antibacterial assays and cultured in nutrient broth (NB) medium at 37 °C overnight with 200 revolutions per minute shaking. The bacterial suspension was diluted to a concentration of 10⁵ CFU/mL with 1/100 NB, and 160 μL of the bacterial suspension was dropped onto each sample and incubated at 37°C under darkness. The samples were sterilized by autoclaving at 121°C for 30 min and placed on 12-well plates before the assays.

Plate count method. The plate count method was used according to a Japanese Industrial Standard (JIS Z 2801-2000). After 24 h of incubation with the bacterial suspension, all samples were washed using phosphate-buffered saline (PBS) and ultrasonically agitated to collect both the non-adherent and adherent bacteria. Then, the bacteria were quantified by standard serial dilution and plate counting to evaluate the antibacterial ability. The formula used to calculate the ARs was as follows: $AR = (A - B)/A \times 100\%$, where A and B represent the average number of bacterial colonies on the cp-Ti sample and the average number of bacterial colonies on the experiment samples, respectively.

Fluorescence staining. After incubation for 24 h, PBS was used to rinse the sample surfaces twice to remove the non-adherent bacteria. The adherent bacteria on samples were stained with SYTO 9 and propidium iodide (PI) (LIVE/DEAD BacLight Bacterial Viability Kits, Life Technologies, USA) for 15 min in darkness and observed by fluorescence microscopy (IX71, Olympus Corporation, Japan).

Bacterial morphology. After sample incubation for 24 h, PBS was used to rinse the sample surfaces twice to remove the non-adherent bacteria. The adherent bacteria were fixed with 2.5% glutaraldehyde (Solarbio, China), dehydrated in gradient ethanol, dried and observed by FE–SEM (S4800, Hitachi, Japan).

In vitro biocompatibility assays

Cell culture. MC3T3-E1 mouse preosteoblasts (Chinese Academy of Sciences Shanghai Cell Bank) were cultured in α -MEM medium (HyClone, USA) with 10% foetal bovine serum (Gemini, Australia) and 1% penicillin–streptomycin and cultured in an incubator with 5% CO₂ at 37°C. The samples were placed in 24-well plates; 1 mL of preosteoblast suspension with 2×10^4 cells/mL was then seeded into each well for cell adhesion and proliferation assays, and 1 mL of preosteoblast suspension with 4×10^4 cells/mL was seeded

into each well for alkaline phosphatase (ALP) assays. The samples were sterilized by autoclaving at 121°C for 30 min before the assays.

Cell adhesion and proliferation. After culturing for 1 and 2h, the sample surfaces were rinsed twice with PBS. The cells were fixed with paraformaldehyde (4%) for 10 min and then permeabilized via treatment with 0.5% Triton X-100 (Solarbio, China) for 5 min. Afterwards, the cells were stained with fluorescein isothiocyanatephalloidin (100 nM, Solarbio, China) and DAPI (100 nM, 6-diamidino-2-phenylindole). Each sample was examined by fluorescence microscopy (IX71, Olympus Corporation, Japan). The number of adherent cells was determined by DAPI staining, and the cells were counted in randomly selected fields using a fluorescence microscope at $100 \times \text{magnification}$. After culture for 1, 3 and 7 days, Cell Counting Kit-8 (CCK-8, Dojindo, Japan) was used to evaluate cell proliferation. The formula used to calculate the relative growth rate (RGR) was as follows: $RGR = OD_{sample}/OD_{cp-Ti} \times 100\%$. RGR values >70% were considered noncytotoxic according to the standard ISO 10993-5.25

ALP assay. After three days of culture in complete culture medium, an additional $10 \,\mathrm{mM}$ β -glycerophosphate and $50 \,\mu\mathrm{g/mL}$ ascorbic acid were supplied to the medium for osteogenic induction. After three and seven days of osteogenic induction, the cells were rinsed and lysed in cell lysis buffer for Western blot analysis and an immunoprecipitation assay without inhibitors (Beyotime, China). The ALP activity in the lysis solution was measured using an ALP Assay Kit (Beyotime, China) based on p-nitrophenyl phosphate. The final results were normalized to the intracellular total protein content determined by an Enhanced BCA Protein Assay Kit (Beyotime, China).

Statistical analysis

The results are expressed as the mean \pm standard deviation. One-way analysis of variance followed by the Student–Newman–Keuls post hoc test was used for statistical analysis. Differences were regarded as significant for p < 0.05, and differences were regarded as highly significant for p < 0.01.

Results

Surface characterization

The surface morphologies of the Ti (AE), Ti–Ag (AE), Ti (CT) and Ti–Ag (CT) samples are shown in Figure 1. Under low magnification, there were micro- and submicroscale pits on the samples modified with acid etching

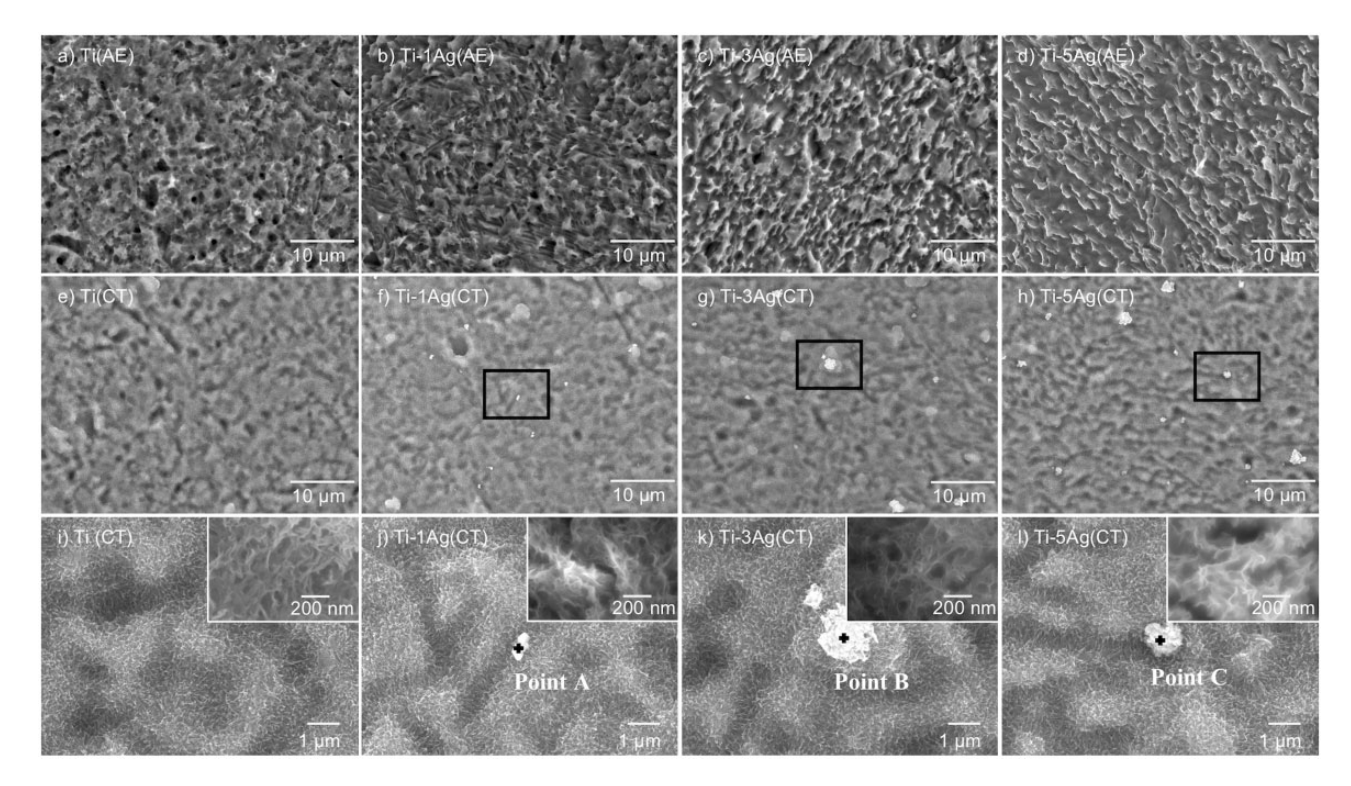


Figure 1. The surface morphologies of the Ti (AE), Ti-Ag (AE), Ti (CT) and Ti-Ag (CT) samples.

and CT. The Ti-Ag (CT) samples had micro- and submicroscale white particles on their surfaces, whereas the Ti (AE), Ti-Ag (AE) and Ti (CT) samples did not have those particles. The results indicated that no particles were immediately formed after acid etching; particle formation occurred upon alkaline treatment after acid etching. Moreover, the Ti-3Ag (AE) and Ti-5Ag (AE) samples possessed more and larger particles on their surfaces than the Ti-1Ag (AE) sample, indicating that the Ag concentration in the Ti-Ag alloys had an effect on the amount and size of particles produced after CT. Under high magnification, the samples modified with CT showed homogenous nanoscale sponge-like structures at the bases of the hybrid micro- and submicroscale pits. This indicated that the micro- and submicroscale pits were acid etched, whereas the nanostructures were ascribed to alkaline treatment.

Figure 2 and Table 1 show the surface chemical composition and the elemental composition of particles determined by EDS. In addition to titanium and silver, oxygen and sodium were observed on the chemically treated samples; the presence of oxygen and sodium was due to the alkaline treatment. Colour mapping images of the Ag distribution are shown in Figure 2, and Table 1 shows the Ag content locations of the particles. As shown in Figure 2 and Table 1, Ag was homogenously distributed on the surfaces of the Ti–Ag (AE) samples, whereas the distribution of Ag on the surfaces of Ti–Ag (CT) samples tended to aggregate

and was not as homogenous as those on the Ti–Ag (AE) samples. Moreover, the Ag contents of the particles on the Ti–Ag (CT) samples were significantly higher than those of the substrate. In general, these results indicated that the alkali treatment made uniformly distributed Ag in the Ti–Ag (AE) aggregate and form particles; these particles on the surfaces of Ti–Ag (CT) samples shown in Figure 1 contained high concentrations of Ag compared with the matrix, which were the high-Ag-content particles.

XRD patterns of the chemically treated samples (Figure 3) show only a-Ti and TiH₂ peaks. Unfortunately, no Ag-related diffraction peaks were detected. The TiH₂ phase resulted from the acid etching.²⁶ The alkali titanate hydrogen layer produced by the interaction of Ti and NaOH is not shown. However, the EDS results of the chemically treated samples confirmed the presence of Na, O and Ti, as shown in Table 1.²⁰

Figure 4 shows 3 D topography images of the samples indicating that CT resulted in porous structures on the surfaces of the Ti (CT) and Ti–Ag (CT) samples, which was consistent with the results shown in Figure 1. Table 2 and Figure 5 show the average roughness (Ra), rootmean-square deviation (Rq) and peak-to-valley roughness (Rz). Compared with the cp-Ti sample, the chemically treated samples had significantly greater roughness (p < 0.01). The Ti (CT) sample had the highest roughness (p < 0.01) among the chemically treated samples. These

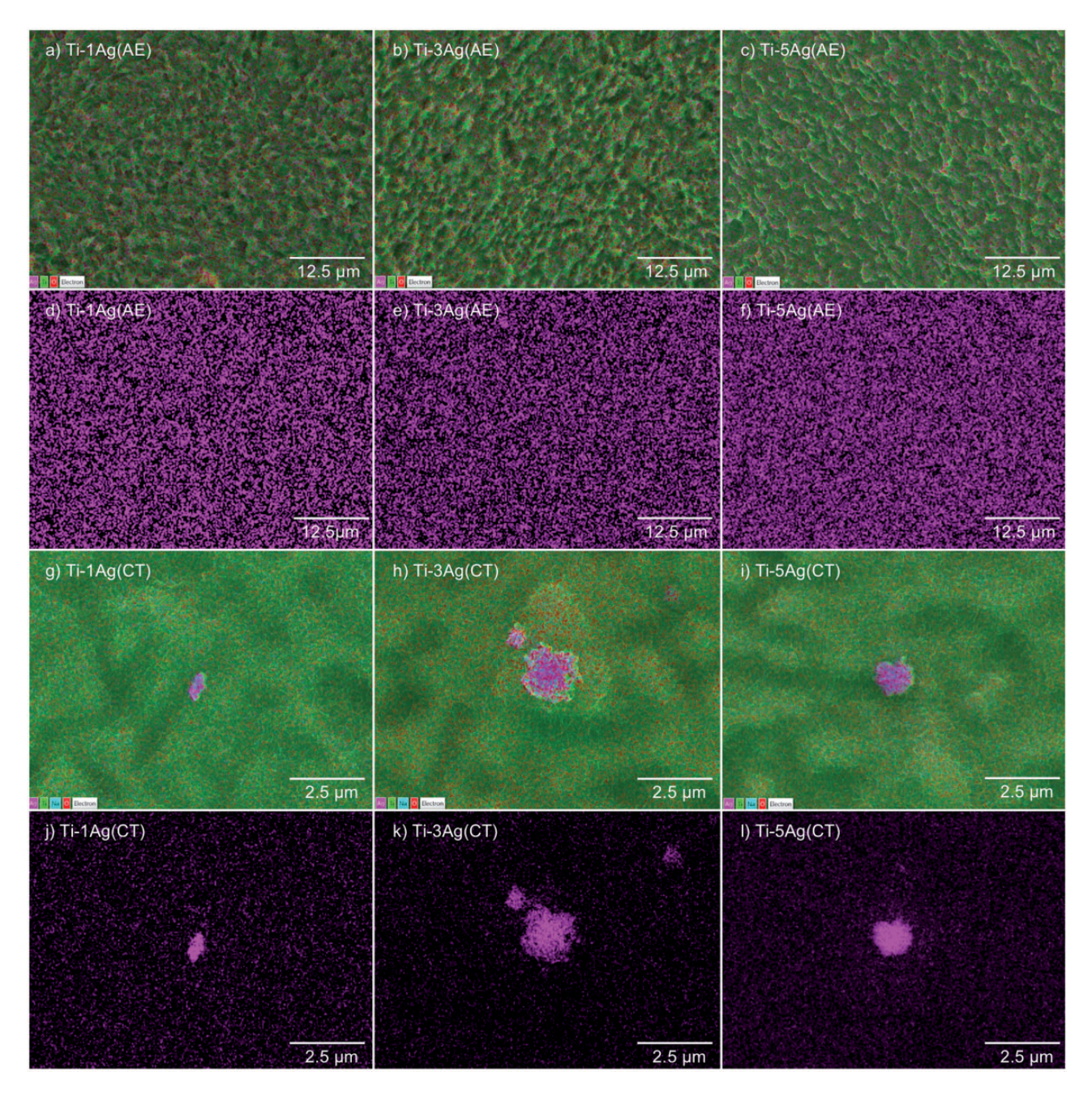


Figure 2. Element mapping of the Ti (AE), Ti–Ag (AE), Ti (CT) and Ti–Ag (CT) samples. (a–c) Ag, Ti and O element mapping, (g–i) Ag, Ti, Na and O element mapping and (d–f) (j–l) Ag element mapping. Ag, Ti, Na and O elements are marked in pink, green, blue and red, respectively.

results indicated that the surface roughness of the samples could be significantly increased by CT, whether those were cp-Ti or Ti-Ag alloys.

As shown in Figure 6, water contact angles were determined to compare the surface hydrophilicity. The samples with CT had significantly higher surface hydrophilicity than the cp-Ti sample (p < 0.01). The differences among the chemically treated samples were not significant (p > 0.05), but hydrophilicity decreased with increasing Ag content. The results

indicated that the surface hydrophilicity of the cp-Ti and Ti-Ag alloys could be increased by CT, which were similar to the previous study.²¹

The concentrations of Ag ions released on days 1, 4, 7, 14 and 28 are shown in Figure 7(a), which indicate that the release of Ag ions increased with increasing Ag content. After one day of immersion, the concentrations of Ag ions released from the Ti-1Ag (CT), Ti-3Ag (CT) and Ti-5Ag (CT) samples were 21.20 ± 4.92 , 45.37 ± 4.56 and 145.17 ± 11.70 ppb,

Table 1.	Surface chemical composition of the cp-Ti, Ti (CT) and			
Ti-Ag (CT) samples.				

	Element (wt.%)				
Samples	Ti	Ag	0	Na	
cp-Ti	92.27	_	7.73	_	
Ti (CT)	70.69	_	28.73	0.58	
Ti-Ì Ag (CT)	69.75	0.75	28.80	0.71	
Ti-3Ag (CT)	67.64	1.90	29.68	0.77	
Ti-5Ag (CT)	67.22	3.35	28.72	0.71	
Point A	43.02	29.80	26.37	0.80	
Point B	29.24	51.30	18.89	0.57	
Point C	30.32	49.94	19.13	0.61	

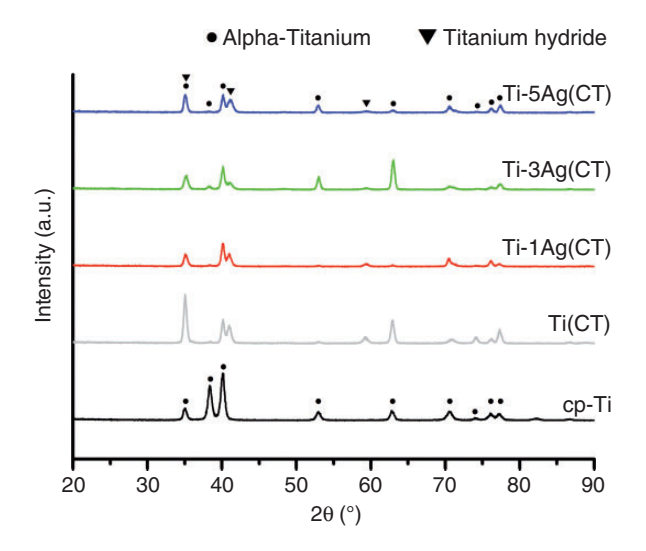


Figure 3. XRD patterns of the cp-Ti, Ti (CT) and Ti–Ag (CT) samples.

respectively. Relatively, large amounts of Ag ions were released on day 1; subsequently, the amount diminished until reaching a steady value after seven days. This result indicated that Ag ion release was greatest on day 1, and the Ag ion release amounts at other times were lower. The pH values of the immersion solutions of the cp-Ti, Ti (CT) and Ti-Ag (CT) samples ranged from 6 to 7, as shown in Figure 7(b). The chemically treated samples had higher, but not significantly higher (p>0.05) pH values than the cp-Ti sample. Additionally, no significant difference in pH values was detected (p>0.05) between the Ti (CT) and Ti-Ag (CT) samples. These results indicated that CT did not significantly improve the pH value.

Antibacterial activity

Figure 8 shows *S. aureus* colonies from the cp-Ti, Ti (CT) and Ti–Ag (CT) samples at 24 h after inoculation. There were a large number of bacterial colonies on the

cp-Ti and Ti (CT) samples, and more colonies were present on the Ti (CT) sample than on the cp-Ti sample. In contrast, only small numbers or no bacterial colonies were observed on the Ti-Ag (CT) samples. The AR results are shown in Figure 9. The AR values of the Ti-1Ag (CT), Ti-3Ag (CT) and Ti-5Ag (CT) samples were $99.28\% \pm 0.61\%$, $99.95\% \pm 0.07\%$ and $99.98\% \pm 0.02\%$, respectively. According to the Industry Standard of China SN/T 2399,²⁷ the Ti-1Ag (CT), Ti-3Ag (CT) and Ti-5Ag (CT) samples had strong antibacterial activities due to ARs > 99%. Live/dead staining and bacterial morphology examinations were performed to further confirm the antibacterial properties of the Ti-Ag (CT) samples. In Figure 10 (a) to (e), green represents the live bacteria, whereas red represents the dead bacteria. There was a large quantity of viable bacteria on the cp-Ti sample and larger quantities on the Ti (CT) sample. In contrast, there were far fewer live bacteria and more dead bacteria on the Ti-Ag (CT) samples than on the other samples. S. aureus bacterial morphologies on the samples at 24 h incubation are shown in Figure 10(f) to (j). There were a large number of bacteria with spherical shapes conglomerating into grapelike colonies on the cp-Ti sample, and more bacteria were present on the Ti (CT) sample. However, only a few scattered bacteria with irregular and broken shapes were observed on the Ti-Ag (CT) samples, indicating that the Ti-Ag (CT) samples could inhibit bacterial colonization and even promote bacterial rupture. The determined bacterial morphologies agreed with the results obtained by the plate count method and fluorescence staining.

Cell response

Figure 11 shows the number of adherent cells on all samples for 1 and 2h cultures. More cells adhered on the samples with CT than on the cp-Ti samples (p < 0.05). Moreover, the difference between the cell numbers of the Ti (CT) and Ti-Ag (CT) samples was not significant (p > 0.05). The morphologies of the cells at 1 and 2h are presented in Figure 12. Compared with the morphologies of the adherent cells on the cp-Ti sample, the morphologies of the adherent cells on the Ti (CT) and Ti-Ag (CT) samples exhibited more cytoplasmic extensions with more filopodia and lamellipodia. The cell proliferation results are shown in Figure 13(a), and the differences among the cp-Ti, Ti (CT) and Ti-Ag (CT) samples for one, three and seven day cultures were not significant (p > 0.05). However, the proliferation capacity of the cp-Ti sample was generally greater than those of the chemically treated samples other than the Ti-5Ag (CT) sample on day 1. These results demonstrated that the Ti (CT) and Ti-Ag (CT) samples promoted the initial adhesion of the cells without promoting cell

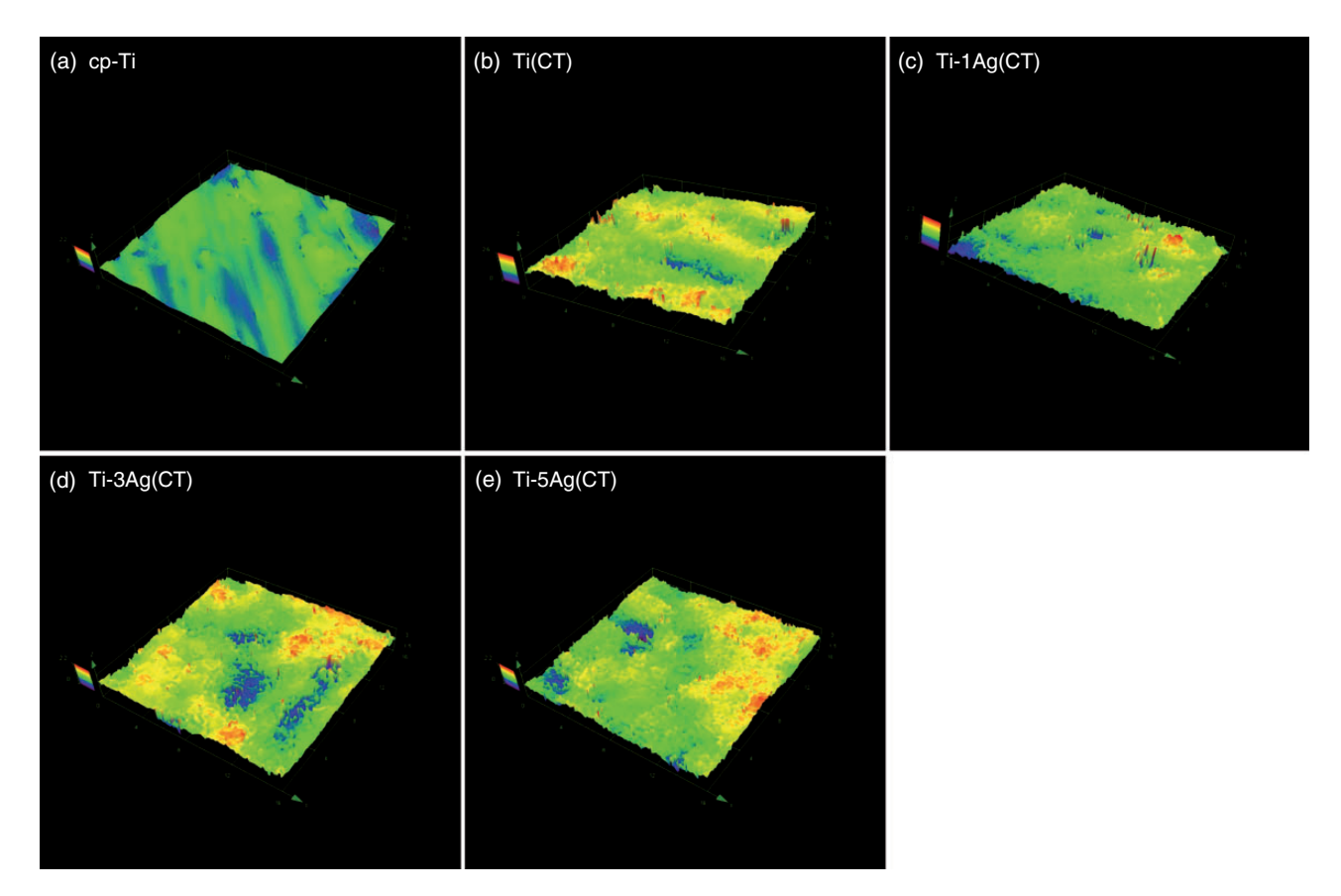


Figure 4. Effect of CT on 3 D topography images of the surfaces of the cp-Ti, Ti (CT) and Ti-Ag (CT) samples.

Table 2. Effect of CT on surface roughness of the cp-Ti, Ti (CT) and Ti–Ag (CT) samples.

Sample	Ra (μm)	Rq (μm)	Rz (μm)
cp-Ti	$\textbf{0.152} \pm \textbf{0.008}$	$\textbf{0.199} \pm \textbf{0.010}$	1.716 ± 0.197
Ti (CT)	$\textbf{0.271} \pm \textbf{0.024}$	$0.343\pm0.03l$	$\textbf{2.647} \pm \textbf{0.279}$
Ti-IAg (CT)	$\textbf{0.245} \pm \textbf{0.022}$	$\textbf{0.311} \pm \textbf{0.025}$	$\textbf{2.503} \pm \textbf{0.179}$
Ti-3Ag (CT)	$\textbf{0.249} \pm \textbf{0.008}$	$\textbf{0.316} \pm \textbf{0.013}$	$\textbf{2.460} \pm \textbf{0.226}$
Ti-5Ag (CT)	$\textbf{0.245} \pm \textbf{0.014}$	$\textbf{0.311} \pm \textbf{0.015}$	$\textbf{2.366} \pm \textbf{0.154}$

proliferation. Moreover, the RGR values of the Ti (CT) and Ti–Ag (CT) samples were all greater than 70%, as shown in Table 3, suggesting that the Ti (CT) and Ti–Ag (CT) samples were noncytotoxic.

ALP is an important early marker for osteogenic differentiation. ²⁸ Figure 13(b) shows that the ALP level increased with increasing induction time. After osteogenic induction for three days, although the differences among the cp-Ti, Ti (CT) and Ti–Ag (CT) samples were not significant (p > 0.05), the ALP activity of the chemically treated samples was generally greater than that of the cp-Ti sample. The ALP activities of the Ti (CT), Ti-1Ag (CT) and Ti-3Ag (CT) samples trended higher than that of the cp-Ti sample (p < 0.05) after osteogenic induction for seven days.

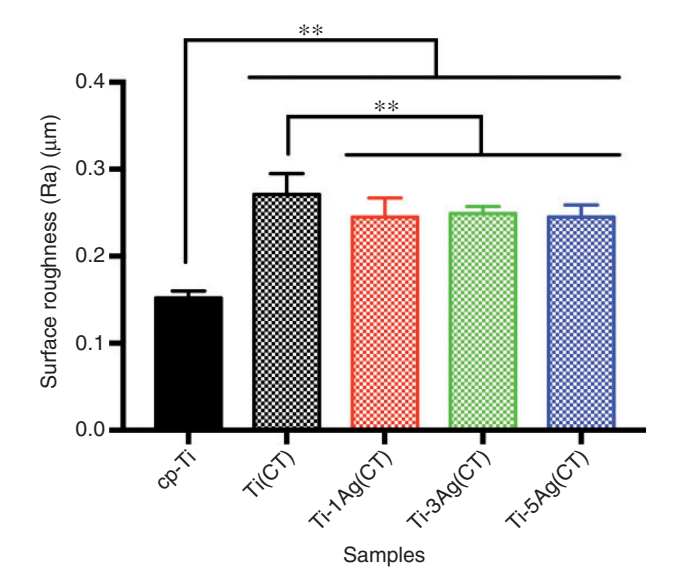


Figure 5. Effect of CT on surface roughness (Ra) of the cp-Ti, Ti (CT) and Ti–Ag (CT) samples. **p < 0.01.

These results indicated that Ti (CT), Ti-1Ag (CT) and Ti-3Ag (CT) enhanced osteoblast differentiation and exhibited osteoinductive properties, and the Ti-5Ag (CT) sample did not impair osteoblast differentiation.

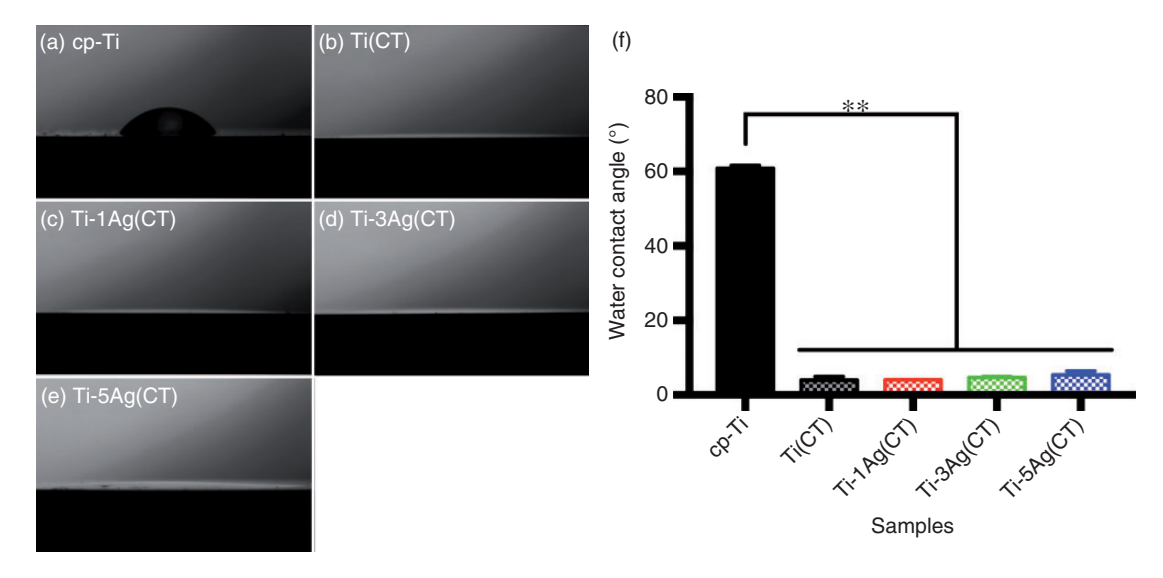


Figure 6. Effect of CT on water contact angles of the cp-Ti, Ti (CT) and Ti–Ag (CT) samples. **p < 0.01.

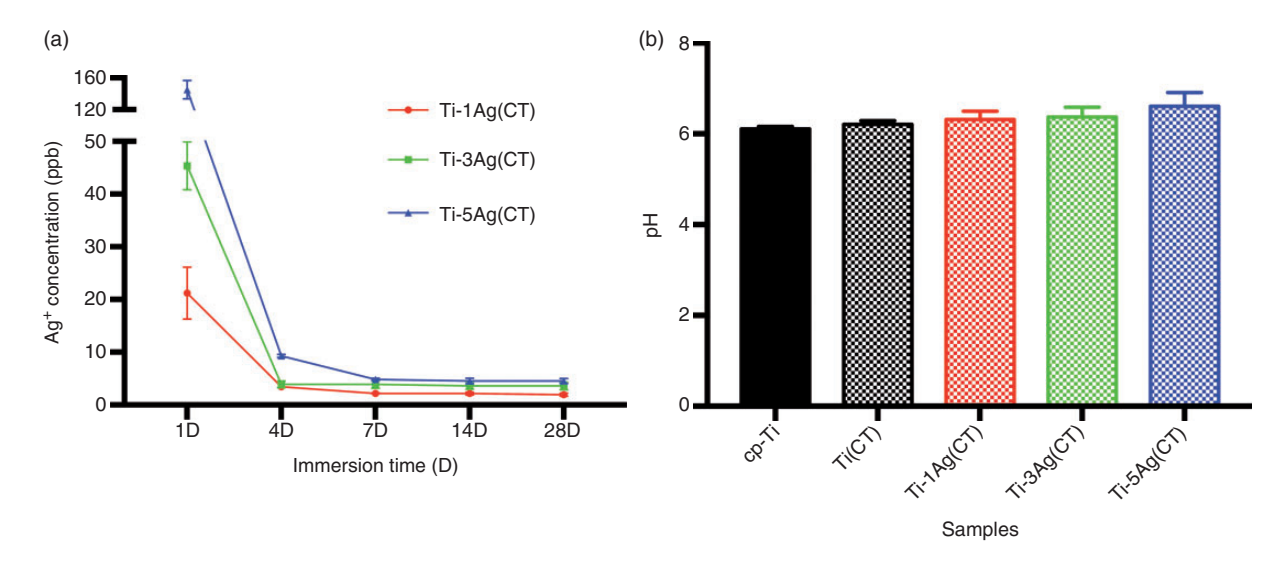


Figure 7. (a) Concentrations of Ag ions released from the Ti–Ag (CT) samples at days 1, 4, 7, 14 and 28; (b) effect of CT on pH values of the cp-Ti, Ti (CT) and Ti–Ag (CT) samples; 0.9% NaCl solution: $pH = 6.13 \pm 0.10$.



Figure 8. Photographs showing S. aureus colonies from the cp-Ti, Ti (CT) and Ti-Ag (CT) samples after culturing for 24 h.

Discussion

PJI and aseptic loosening are the two main challenges of joint arthroplasty prostheses. Biomaterials that simultaneously prevent PJIs and promote osseointegration are needed. In this study, we supplied Ag as an antibacterial

agent to cp-Ti to prepare a Ti-Ag casting alloy. Afterwards, CT (acid etching plus alkaline treatment) was used to fabricate hybrid micro-, submicro- and nanofeatures on the surface; this method is inexpensive, effective and reproducible and has been confirmed to improve osteoinduction and osseointegration. ^{20,21,29,30}

The initial acid etching resulted in the generation of pits with micro- and submicron features, and alkaline treatment resulted in the generation of a sponge with nanofeatures. Moreover, alkaline treatment resulted in particles with high Ag content that were generated on the surfaces of the samples after acid etching. Similarly, Zhang and Liu³¹ reported that Cu-containing particles formed on the surface of a Ti–Cu-sintered alloy after alkaline heat treatment, and the particles were confirmed to be Ti₂Cu. However, in this study, the phase in the Ag content particle was not identified by EDS or XRD and thus requires further investigation. Moreover, the antibacterial assay results indicated that the high-Agcontent particles played a key role in the antibacterial activities of the Ti–Ag (CT) samples.

The Ti–Ag (CT) samples, even the Ti-1 wt.% Ag after CT, exhibited strong antibacterial activities as confirmed

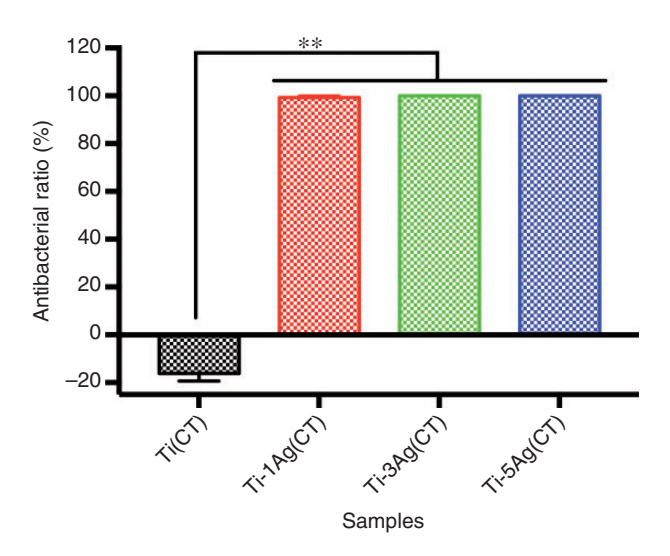


Figure 9. ARs of S. *aureus* cultured on the Ti (CT) and Ti–Ag (CT) samples after culturing for 24 h. **p < 0.01.

by plate counting, fluorescence staining and FE–SEM. It is well known that one of the antibacterial mechanisms of Ag-containing materials is Ag ion release^{32,33} and that Ag ions lead to bacterial protein inactivation, DNA impairment, increased membrane permeability and cellular content leakage.³⁴ Furthermore, Greulich et al.³⁵ found that the minimum inhibitory concentration (MIC) of Ag ions was 2.5–5 ppm when *S. aureus* was cultured in lysogeny broth medium. In this study, the Ag ion concentrations of the Ti–Ag (CT) samples on days 1, 4, 7, 14 and 28 were all lower than the MIC, which demonstrated that the antibacterial activities of Ti–Ag (CT) samples did not completely rely on the Ag ions. Li et al.³⁶ reported that cp-Ti with alkaline treatment showed an antibacterial effect due to increased pH and

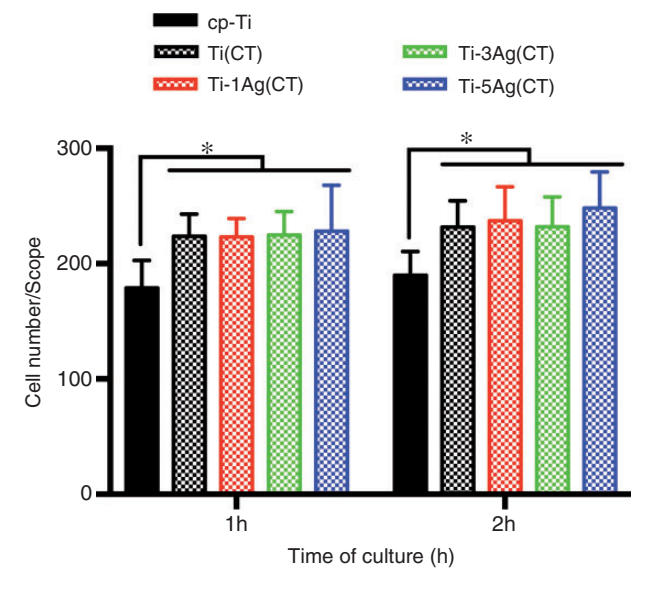


Figure 11. Number of adherent MC3T3-E1 cells on the cp-Ti, Ti (CT) and Ti–Ag (CT) samples after culturing for 1 and 2 h. *p < 0.05.

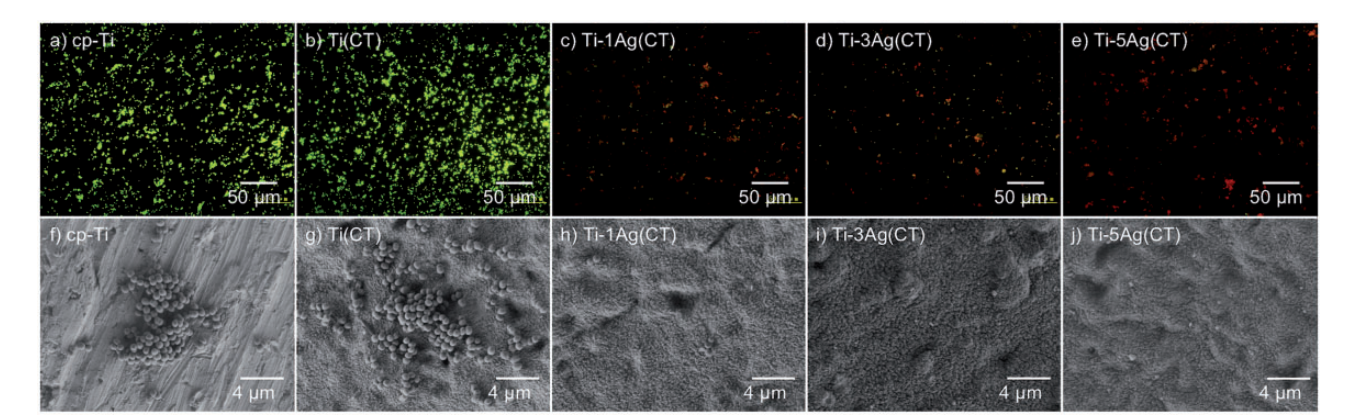


Figure 10. (a–e) Live/dead staining showing S. aureus cultured on the cp-Ti, Ti (CT) and Ti-Ag (CT) samples for 24 h; (f–j) SEM morphology showing S. aureus cultured on the cp-Ti, Ti (CT), and Ti-Ag (CT) samples for 24 h.

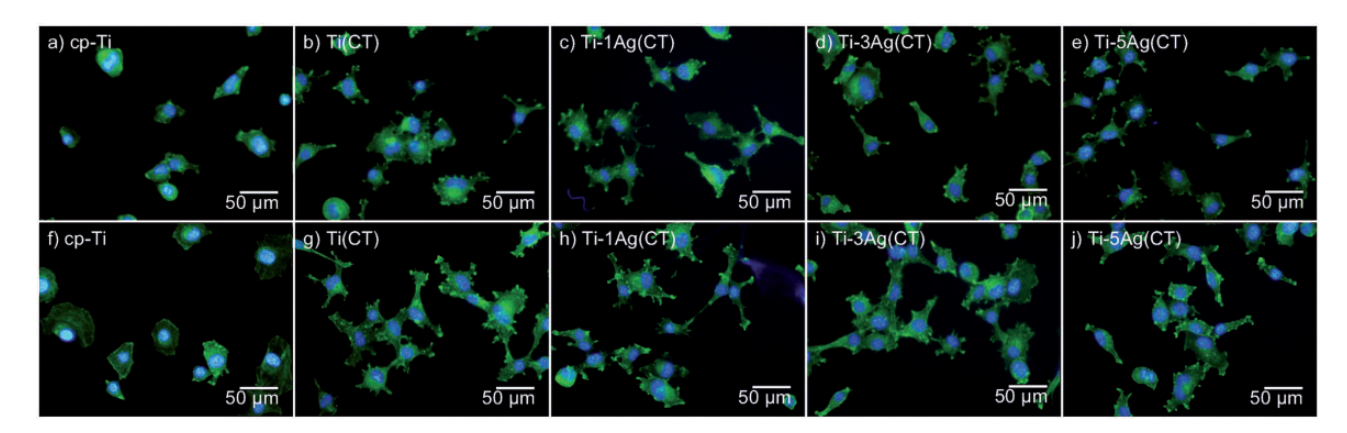


Figure 12. Fluorescent images showing MC3T3-E1 cells that adhered on the cp-Ti, Ti (CT) and Ti-Ag (CT) samples after culturing for 1 and 2 h.

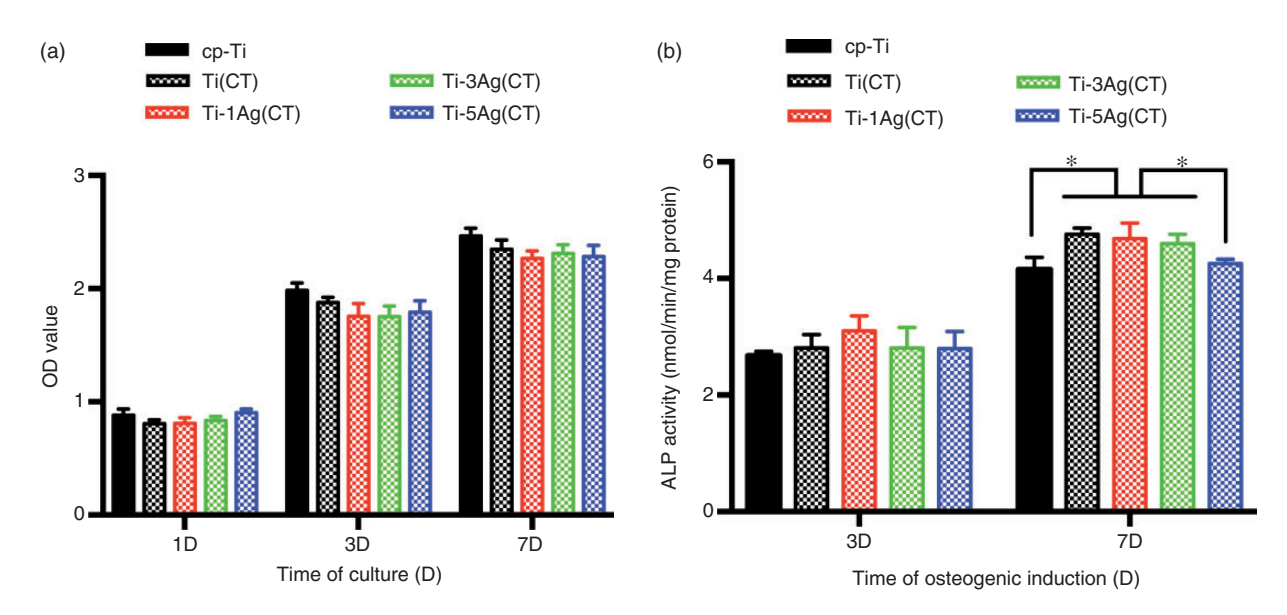


Figure 13. (a) Proliferation of MC3T3-E1 cells on the cp-Ti, Ti (CT) and Ti–Ag (CT) samples after culturing for one, three and seven days; (b) ALP activity of MC3T3-E1 cells cultured on the cp-Ti, Ti (CT) and Ti–Ag (CT) samples after osteogenic induction for seven days. *p < 0.05.

Table 3. RGRs of the cp-Ti, Ti (CT) and Ti-Ag (CT) samples.

Sample	One day	Three days	Seven days
cp-Ti	100%	100%	100%
Ti (CT)	91.25% \pm 3.86%	$94.55\% \pm 2.27\%$	$95.05\% \pm 3.37\%$
Ti-Î Ag (CT)	91.93% \pm 5.68%	$88.55\% \pm 5.65\%$	$91.93\% \pm 2.68\%$
Ti-3Ag (CT)	$94.77\% \pm 3.98\%$	$88.45\% \pm 4.64\%$	$93.67\% \pm 3.16\%$
Ti-5Ag (CT)	$102.73\% \pm 3.52\%$	$90.32\% \pm 5.14\%$	$92.58\% \pm 4.10\%$

micro/nanotopography formation. In this study, the pH value differences between the cp-Ti and chemically treated samples were not statistically significant; all pH values were between 6 and 7, i.e. optimum pH values for *S. aureus* growth,³⁷ demonstrating that the pH values of

the Ti–Ag (CT) samples had little effect on antibacterial activities. In contrast to the results of Li et al.,³⁶ who found that micro/nanotopography inhibited *S. aureus* adhesion and proliferation, the Ti (CT) samples with micro-, submicro- and nanotopography in our study

were more beneficial for S. aureus adhesion and proliferation than the cp-Ti sample because their roughness was higher than that of the machined cp-Ti sample. 38,39 This difference may be attributed to the different control groups. The relatively rough cp-Ti with acid etching was chosen as the control group in Li et al., 36 whereas the relatively smooth cp-Ti sample with 2000 grit SiC paper grinding was chosen as the control group in our study. Kang et al. 15 reported results similar to ours, showing that Ag particles formed on the surfaces of Ti-Ag alloys after grit blasting and acid etching; further, the concentrations of Ag ions released from SLA-treated Ti-Ag alloys were lower than the MIC of Ag ions. Therefore, Kang et al. 15 attributed the antibacterial activities of Ti-Ag alloys to Ag ion release and Ag particles. In our previous study²² and in a study by Chen et al., 12 Ag ion release and direct contact between the Ag-containing particles and bacteria were two antibacterial mechanisms of Ag-containing titanium-based materials. Taking these results together, in addition to Ag ion release, the Ag-containing particles also contributed to the strong antibacterial activities of the Ti-Ag (CT) samples.

The roughness and hydrophilicity of the Ti–Ag (CT) samples were improved by the presence of micro-, submicro- and nanotopography. This special topography has been shown to enhance cellular bioactivity, osteoconduction, osteoinduction and osseointegration. 20,21,29,30,40 Cell adhesion is the first stage of cell/ biomaterial interaction, which influences cell proliferation and differentiation.⁴¹ Cell adhesion is positively but non-linearly correlated with cell proliferation. Cell proliferation capacity was highest when the adhesion strength between the cell and material surface was intermediate.⁴² A similar phenomenon was also observed in our assays: the chemically treated surfaces improved cell adhesion in the initial 1 and 2h, but the proliferation capacity did not improve. Although Ag has been applied in clinical settings as an antibacterial agent, its cytocompatibility remains a concern⁶; Ag ion concentrations below 1.20 ppm have been reported to show no cytotoxicity. 43,44 In this research, the Ag ions released from the Ti-Ag (CT) samples were all below the reported toxicity threshold during the 28-day immersion period. It is worth noting that the RGR values of the Ti (CT) and Ti-Ag (CT) samples were all >70%, indicating that the chemical treatment and/ or Ag (1-5 wt.%) added to the cp-Ti sample were noncytotoxic. The relatively low proliferation capacity of the Ti (CT) and Ti-Ag (CT) samples was also attributed to the differentiation promotion due to the reciprocal relationship between proliferation and differentiation. 16,45 Osteoblast differentiation enhanced by the chemical treatment, indicating that the Ti (CT), Ti-1Ag (CT) and Ti-3Ag (CT) samples had osteoinductive properties and provided an important signal to enhance the osseointegration. 20,46,47 However, the antibacterial activities and osseointegrative properties of the Ti–Ag (CT) samples require further investigation in vivo because the in vivo environment in humans cannot be completely simulated by in vitro experiments.

Conclusions

CT modification on casted Ti–Ag alloys enhanced their antibacterial activity, bioactivity and osteoinduction. Hybrid micron and submicron porosities, sponge-like nanostructures and Ag-containing particles formed on the surfaces of the Ti–Ag alloys after the CT. The Ti-1Ag (CT), Ti-3Ag (CT) and Ti-5Ag (CT) samples showed strong antibacterial activities dependent on Ag ion release and Ag-containing particles. Moreover, the Ti-1Ag (CT) and Ti-3Ag (CT) samples showed better cell responses with respect to adhesion and osteogenic differentiation due to their special topographies.

Declaration of conflicting interests

The author(s) declare no potential conflicts of interest with respect to the research, authorship, and/or publication of this article.

Funding

The author(s) disclosed receipt of the following financial support for the research, authorship, and/or publication of this article: This work was supported by the National Natural Science Foundation of China (81671811, 81501857), the Special Research Foundation of the Health and Family Planning Commission of Liaoning Province (LNCCC-A03-2014), and the Science and Technology Project of Shenyang City (17-230-9-09, F16-206-9-21).

ORCID iD

Xizhuang Bai https://orcid.org/0000-0002-9338-8643

References

- 1. Chen Q and Thouas GA. Metallic implant biomaterials. *Mater Sci Eng R: Rep* 2015; 87: 1–57.
- Voigt J, Mosier M and Darouiche R. Systematic review and meta-analysis of randomized controlled trials of antibiotics and antiseptics for preventing infection in people receiving primary total hip and knee prostheses. Antimicrob Agents Chemother 2015; 59: 6696–6707.
- 3. Sadoghi P, Liebensteiner M, Agreiter M, et al. Revision surgery after total joint arthroplasty: a complication-based analysis using worldwide arthroplasty registers. *J Arthroplast* 2013; 28: 1329–1332.
- 4. Arciola CR, Campoccia D, Speziale P, et al. Biofilm formation in *Staphylococcus* implant infections: a review of

molecular mechanisms and implications for biofilm-resistant materials. *Biomaterials* 2012; 33: 5967–5982.

- Apostu D, Lucaciu O, Berce C, et al. Current methods of preventing aseptic loosening and improving osseointegration of titanium implants in cementless total hip arthroplasty: a review. J Int Med Res 2017; 46: 2104–2119.
- Chernousova S and Epple M. Silver as antibacterial agent: ion, nanoparticle, and metal. Angew Chem Int Ed Engl 2013: 52: 1636–1653.
- Qin H, Cao H, Zhao Y, et al. Antimicrobial and osteogenic properties of silver-ion-implanted stainless steel. ACS Appl Mater Interf 2015; 7: 10785–10794.
- 8. Duran N, Duran M, de Jesus MB, et al. Silver nanoparticles: a new view on mechanistic aspects on antimicrobial activity. *Nanomedicine* 2016; 12: 789–799.
- Ferraris S and Spriano S. Antibacterial titanium surfaces for medical implants. *Mater Sci Eng C Mater Biol Appl* 2016; 61: 965–978.
- Wafa H, Grimer RJ, Reddy K, et al. Retrospective evaluation of the incidence of early periprosthetic infection with silver-treated endoprostheses in high-risk patients. *Bone Joint J* 2015; 97B: 252–257.
- Nakajo K, Takahashi M, Kikuchi M, et al. Inhibitory effect of Ti-Ag alloy on artificial biofilm formation. *Dent Mater J* 2014; 33: 389–393.
- Chen M, Yang L, Zhang L, et al. Effect of nano/micro-Ag compound particles on the bio-corrosion, antibacterial properties and cell biocompatibility of Ti-Ag alloys. *Mater Sci Eng C Mater Biol Appl* 2017; 75: 906–917.
- Chen M, Zhang E and Zhang L. Microstructure, mechanical properties, bio-corrosion properties and antibacterial properties of Ti-Ag sintered alloys. *Mater Sci Eng C Mater Biol Appl* 2016; 62: 350–360.
- 14. Cochran DL, Jackson JM, Bernard JP, et al. A 5-year prospective multicenter study of early loaded titanium implants with a sandblasted and acid-etched surface. *Int J Oral Maxillofac Implants* 2011; 26: 1324–1332.
- 15. Kang M-K, Moon S-K, Kwon J-S, et al. Antibacterial effect of sand blasted, large-grit, acid-etched treated Ti-Ag alloys. *Mater Res Bull* 2012; 47: 2952–2955.
- 16. Gittens RA, McLachlan T, Olivares-Navarrete R, et al. The effects of combined micron-/submicron-scale surface roughness and nanoscale features on cell proliferation and differentiation. *Biomaterials* 2011; 32: 3395–3403.
- 17. Li Y, Wang W, Liu H, et al. Formation and in vitro/in vivo performance of "cortex-like" micro/nano-structured TiO₂ coatings on titanium by micro-arc oxidation. *Mater Sci Eng C Mater Biol Appl* 2018; 87: 90–103.
- 18. Zhao G, Raines AL, Wieland M, et al. Requirement for both micron- and submicron scale structure for synergistic responses of osteoblasts to substrate surface energy and topography. *Biomaterials* 2007; 28: 2821–2829.
- 19. Zhao G, Zinger O, Schwartz Z, et al. Osteoblast-like cells are sensitive to submicron-scale surface structure. *Clin Oral Implant Res* 2006; 17: 258–264.
- 20. Zhao C, Zhu X, Liang K, et al. Osteoinduction of porous titanium: a comparative study between acid-alkali and chemical-thermal treatments. *J Biomed Mater Res Part B Appl Biomater* 2010; 95: 387–396.

- 21. Oliveira DP, Palmieri A, Carinci F, et al. Gene expression of human osteoblasts cells on chemically treated surfaces of Ti-6Al-4V-ELI. *Mater Sci Eng C Mater Biol Appl* 2015; 51: 248–255.
- 22. Lei Z, Zhang H, Zhang E, et al. Antibacterial activities and biocompatibilities of Ti-Ag alloys prepared by spark plasma sintering and acid etching. *Mater Sci Eng C Mater Biol Appl* 2018; 92: 121–131.
- 23. 10993-12. ISO Biological evaluation of medical devices: sample preparation and reference materials, 2012.
- 24. 2801 JIS Z. Antimicrobial products-Test for antimicrobial activity and efficacy, 2000.
- 25. 10993-5 ISO. Biological evaluation of medical devices: tests for in vitro cytotoxicity, 2009.
- 26. Lin X, Zhou L, Li S, et al. Behavior of acid etching on titanium: topography, hydrophility and hydrogen concentration. *Biomed Mater* 2014; 9: 015002–012013.
- 2399 SN/T. Evaluation method for antimicrobial metallic materials. 2010.
- 28. Cheng H, Xiong W, Fang Z, et al. Strontium (Sr) and silver (Ag) loaded nanotubular structures with combined osteoinductive and antimicrobial activities. *Acta Biomater* 2016; 31: 388–400.
- Oliveira DP, Palmieri A, Carinci F, et al. Osteoblasts behavior on chemically treated commercially pure titanium surfaces. *J Biomed Mater Res A* 2014; 102: 1816–1822.
- 30. Mendonca G, Mendonca DB, Aragao FJ, et al. Advancing dental implant surface technology from micronto nanotopography. *Biomaterials* 2008; 29: 3822–3835.
- Zhang E and Liu C. Effect of surface treatments on the surface morphology, corrosion property, and antibacterial property of Ti-10Cu sintered alloy. *Biomed Mater* 2015; 10: 045009.
- 32. Zhang X, Wu H, Geng Z, et al. Microstructure and cytotoxicity evaluation of duplex-treated silver-containing antibacterial TiO₂ coatings. *Mater Sci Eng C Mater Biol Appl* 2014; 45: 402–410.
- 33. Huang Y, Zhang X, Zhang H, et al. Fabrication of silverand strontium-doped hydroxyapatite/TiO₂ nanotube bilayer coatings for enhancing bactericidal effect and osteoinductivity. *Ceram Int* 2017; 43: 992–1007.
- 34. Ovington LG. The truth about silver. *Ostomy Wound Manage* 2004; 50(9A Suppl): 1S–10S.
- 35. Greulich C, Braun D, Peetsch A, et al. The toxic effect of silver ions and silver nanoparticles towards bacteria and human cells occurs in the same concentration range. *RSC Adv* 2012; 2: 6981–6987.
- Li J, Wang G, Wang D, et al. Alkali-treated titanium selectively regulating biological behaviors of bacteria, cancer cells and mesenchymal stem cells. *J Colloid Interf Sci* 2014; 436: 160–170.
- Medveov A and Valk U. Staphylococcus aureus: characterisation and quantitative growth description in milk and artisanal raw milk cheese production. Struct Funct Food Eng. Epub ahead of print 22 August 2012. DOI: 10.5772/48175.
- 38. Katsikogianni M and Missirlis YF. Concise review of mechanisms of bacterial adhesion to biomaterials and

- of techniques used in estimating bacteria-material interactions. *Eur Cell Mater* 2004; 8: 37–57.
- 39. Scheuerman TR, Camper AK and Hamilton MA. Effects of substratum topography on bacterial adhesion. *J Colloid Interface Sci* 1998; 208: 23–33.
- 40. Agarwal R and Garcia AJ. Biomaterial strategies for engineering implants for enhanced osseointegration and bone repair. *Adv Drug Deliv Rev* 2015; 94: 53–62.
- 41. Anselme K. Osteoblast adhesion on biomaterials (Review). *Biomaterials* 2000; 21: 667–681.
- 42. Bacakova L, Filova E, Parizek M, et al. Modulation of cell adhesion, proliferation and differentiation on materials designed for body implants. *Biotechnol Adv* 2011; 29: 739–767.
- 43. Tweden KS, Cameron JD, Razzouk AJ, et al. Biocompatibility of silver-modified polyester for

- antimicrobial protection of prosthetic valves. *J Heart Valve Dis* 1997; 6: 553–561.
- 44. Hardes J, Streitburger A, Ahrens H, et al. The influence of elementary silver versus titanium on osteoblasts behaviour in vitro using human osteosarcoma cell lines. *Sarcoma* 2007; Article ID 26539.
- 45. Zhao L, Liu L, Wu Z, et al. Effects of micropitted/nano-tubular titania topographies on bone mesenchymal stem cell osteogenic differentiation. *Biomaterials* 2012; 33: 2629–2641.
- Lopez M, Bassi MA, Confalone L, et al. Titanium disk surfaces modulate dental implants osseointegration. Eur J Inflamm 2012; 10: 43–47.
- 47. Albrektsson T and Johansson C. Osteoinduction, osteoconduction and osseointegration. *Eur Spine J* 2001; 10: S96–S101.